Opposite photo-induced deformations in azobenzene-containing polymers with different molecular architecture: Molecular dynamics study

Jaroslav M. Ilnytskyi,[1,a)] Dieter Neher,[2] and Marina Saphiannikova[3]
[1]*Institute for Condensed Matter Physics of National Academy of Sciences of Ukraine, 1, Svientsitskii Str., 79011 Lviv, Ukraine*
[2]*Institute for Physics and Astronomy, University of Potsdam, Karl-Liebknecht-Strasse 24-25, 14476 Potsdam-Golm, Germany*
[3]*Leibniz Institute of Polymer Research Dresden, Hohe Str. 6, 01069 Dresden, Germany*

(Received 27 April 2011; accepted 29 June 2011; published online 26 July 2011)

Photo-induced deformations in azobenzene-containing polymers (azo-polymers) are central to a number of applications, such as optical storage and fabrication of diffractive elements. The microscopic nature of the underlying opto-mechanical coupling is yet not clear. In this study, we address the experimental finding that the scenario of the effects depends on molecular architecture of the used azo-polymer. Typically, opposite deformations in respect to the direction of light polarization are observed for liquid crystalline and amorphous azo-polymers. In this study, we undertake molecular dynamics simulations of two different models that mimic these two types of azo-polymers. We employ hybrid force field modeling and consider only *trans*-isomers of azobenzene, represented as Gay-Berne sites. The effect of illumination on the orientation of the chromophores is considered on the level of orientational hole burning and emphasis is given to the resulting deformation of the polymer matrix. We reproduce deformations of opposite sign for the two models being considered here and discuss the relevant microscopic mechanisms in both cases. © *2011 American Institute of Physics*. [doi:10.1063/1.3614499]

I. INTRODUCTION

The role played by azobenzene-containing polymers (azo-polymers) in the modern photonic, electronic, and opto-mechanical applications cannot be underestimated. These polymers are successfully used to produce alignment layers for liquid crystalline fluorescent polymers in the display and semiconductor technology,[1,2] to build waveguides and waveguide couplers,[3,4] as data storage media,[5–8] labels in quality product protection,[9] and in a number of other applications. A hot topic in modern research is light-driven artificial muscles based on azobenzene elastomers.[10–13]

A number of extensive reviews that are focused on various properties of azobenzene and azobenzene-containing materials are available.[3,14–17] Therefore, we will recall briefly principal features that are relevant to our study. The main property of the azobenzene chromophore is its ability to photoisomerize between prolate *trans*- and bended *cis*-isomers[14,18] (see Fig. 1). Absorbing maxima for *trans-cis* and *cis-trans* transformations can be tuned by substitution groups R, R'. We will consider in this study the case for which absorption curves for the *trans-cis* and *cis-trans* transitions overlap essentially (e.g., NO_2 substituted azobenzene). For such chromophores, a cyclic *trans-cis-trans* photoisomerization can be achieved which leads to the photo-stationary state where both types of isomers coexist.

At ambient conditions *trans*-azobenzene is found in a crystal form, whereas it acts as a mesogen when incorporated into an azo-polymer. We will restrict ourselves to the case of a side-chain molecular architecture, which contains a backbone and pending spacer chains terminated by azobenzene chromophores. Bulk phase behavior of such systems is similar to the case of non-azobenzene containing side-chain liquid crystalline (LC) polymers.[19–21] An important factor in their phase diagram is the amount of coupling between chromophores and the backbone, which is determined by the length of a spacer between the two.

Typically, for the case of a long spacer both subsystems are decoupled and microphase separation into lamellar smectic phase(s) occurs. For instance, for the siloxane side-chain LC polymer, one or several smectic phases are observed at the spacer length of six and more methylene groups. With the decrease of the spacer length, the coupling between two subsystems increases, and either nematic (for the spacer of 3–5 groups) or even no LC phases (for the spacer of two or less groups) are found.[19] Other factors (transient dipole moment, steric effects, etc.) may also affect the phase behavior.[19–21] Commonly, the side-chain azo-polymers are split into the LC and amorphous systems, the names are self-explanatory.

Due to photosensitivity of azobenzene groups, the degree of LC order in side-chain azo-polymers can be manipulated by suitable illumination. The first effect to mention is the reduction of the LC order, formed by *trans*-isomers in ordered LC phase, by non-mesogenic *cis*-isomers (the so-called photo-chemical transition).[17,22–24] The second effect, much exploited after the seminal work by Eich *et al.*,[25] is the reorientation of *trans*-isomers predominantly perpendicularly to the light polarization (the so-called orientational hole burning).[26,27] Photo-induced reorientation of azobenzenes is known to take place in both LC (Refs. 15, 23, and 24) and

a)Electronic mail: iln@icmp.lviv.ua.

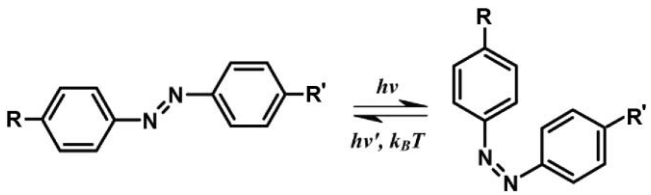

FIG. 1. The photoisomerization of azobenzene chromophores.

amorphous azo-polymers.[20,28,29] These effects enable fabrication of azo-polymer based phase gratings, in which orientation of the chromophores is spatially modulated.[23]

Photo-induced changes in LC order of chromophores in azo-polymers generate internal stress in the material, which (if the film is not jammed between substrates) can be relaxed via flow or deformation of the sample. The exact microscopic mechanism depends on the details of polymer molecular architecture. This was clearly demonstrated by Bublitz *et al.* via illumination of free-floating azo-polymer droplets with the uniform linearly polarized beam. In the case of P6a12 polymer (the molecular architecture with long side spacer), the droplet was found to contract along the polarization vector. In contrary, in the case of E1aP polymer (with short spacer and the backbone that incorporates aromatic rings) the droplet was found to extend along the polarization vector.[30] These findings are closely related to the bending of azobenzene containing elastomer when illuminated.[11,13] In yet another experiment, a linearly polarized beam was applied through an optical mask with light stripes. In this case either hills or trenches were observed in illuminated areas, again, depending on the details of the polymer.[31] Under spatially modulated illumination (holographic-like setup) the even more striking effect of surface relief grating (SRG) formation was discovered in 1995,[32,33] which received considerable attention since then.[3,14,16,17]

The SRG can be inscribed in both LC and amorphous azo-polymers (for reviews, see Refs. 3, 14 and 17). The effect is puzzling in the way that SRG formation takes place in amorphous azo-polymers well below the glass transition temperature T_g. Several models[14,34–40] have been suggested towards the explanation of the origin of the inscribing force but none of them describes satisfactorily the light induced motion of the azobenzene polymers at molecular level.[41,42] Some of them assume a considerable degree of photo-induced plasticization, at least comparable with that at the glass transition. However, only very weak plasticization has been found in mechanical experiments performed recently[43,44] that led to the conclusion that illumination of an azobenzene polymer layer with actinic light cannot induce a transition into a macroscopic low-viscosity melt. A thermodynamic theory valid for amorphous azo-polymer with weak interactions between azobenzenes was developed in Refs. 42 and 45. A number of optical setups can be used to produce the SRG, in particular, the ones utilizing linearly and circularly polarized light (for more details, see review papers[3,14]). Nunzi and co-workers demonstrated that the use of an incoherent light source is also efficient for the deformation of azopolymer nanospheres[46] and for printing a well-organized pattern at the surface of an azopolymer thin film.[47] Here, we focus our attention on the case of a linearly polarized light.

In this study, we exploit several ideas and issues that were suggested and discussed earlier. The first important issue is that both cases of uniform and spatially modulated illumination are related, as the latter can be explained via deformations of small volume elements depending on local intensity and polarization of light (see, e.g., Ref. 39, 42, and 48). Therefore, one can concentrate on microscopic mechanisms for photo-induced deformations that occur in small volume elements. Another important issue is possible increase of the liquid crystallinity due to the reorientation of chromophores. By application of the Maier-Saupe theory[49] it was shown that the sample in this case contracts along the polarization vector.[37]

In this paper, we assume the photo-induced reorientation of the azobenzenes as being a principal initiator of all mechanical changes in the azo-polymer. We concentrate on a "missing link" – the microscopic mechanisms that are responsible for converting these reorientational perturbations into mechanical deformation of the azo-polymer. We perform molecular dynamics (MD) simulations and extend essentially our previous findings.[50–53] In particular, wider interval of reorientating field strengths is considered, the study now includes the cases of a poly-domain smectic sample below the smectic-isotropic transition and of an amorphous sample near glass transition temperature. In general, much longer simulation runs are performed as compared to our previous studies.[50–53] The outline of the paper is as follows. The details of modeling and simulation technique are provided in Sec. II, photo-induced deformations in the model representing LC azo-polymer are presented in Sec. III, the same for the model for the amorphous azo-polymers are given in Sec. IV, conclusions are contained in Sec. V.

II. MODELING AND SIMULATIONAL TECHNIQUE

In this study, we use a hybrid semi-atomistic modeling,[54] which turned out to be an efficient approach for description of the structure, dynamics, and phase transformations in LC polymers.[55] It is a classical mechanical description based on the force field type of modeling, in which polymer beads are interpreted as Lennard-Jones sites and azobenzenes as Gay-Berne[56] sites. The focus is, therefore, on the most relevant features of the LC polymer, namely, the (variable) flexibility of polymer chains and the ability of mesogens to form LC phases.

As follows from the experimental findings,[11,30] the spacer length and the rigidity of the polymer backbone play important role in photo-mechanical response of azo-polymers. Therefore, we construct two models. Both have in common the same backbone length of 39 sites and the same number of 10 pending side chains attached to it in a syndiotactic way, see Fig. 2. However, the models differ in the following details. The weakly coupled model has flexible, alkyl-like backbone and relatively long flexible spacer of ten sites and is aimed to model the LC azo-polymer (e.g., similar to P6a12). It is known that at suitable temperatures it forms a lamellar smectic phase.[57,58] The second, strongly coupled model, has

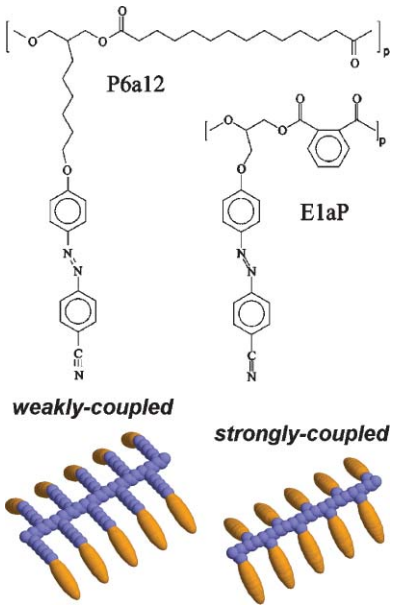

FIG. 2. Chemical structure of P6a12 and E1aP azo-polymers (top frame) and space-filled representation of molecular architecture for the weakly and strongly coupled models (bottom frame).

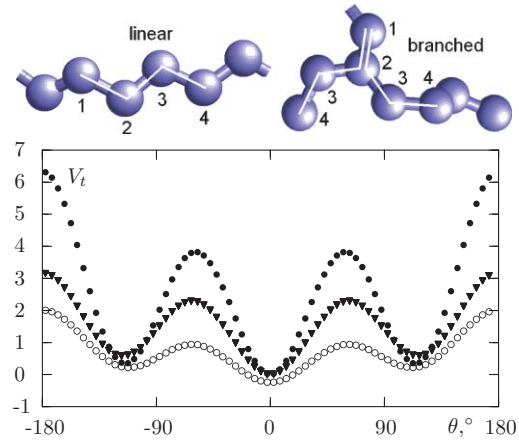

FIG. 3. Top frame – torsion angles in linear and branched fragments of the polymer chain. Bottom frame – the form of the torsion potential (Eq. (1)) for linear (triangles) and branched (open circles) fragments of a polymer chain in weakly coupled model and for all torsion angles in strongly coupled model (filled circles). The units are 10^{-20} J.

a very short spacer of two sites and an increased rigidity of the backbone to mimic main features of E1aP azo-polymer. The rigidity of the backbone is defined by the height of the potential barrier between *trans* and *gauch* conformations of the torsion angle. Torsion potential is defined in a form of Ryckaert and Bellemans[59]

$$V_t = C_0 + C_1 \cos\theta + C_2 \cos^2\theta + C_3 \cos^3\theta. \quad (1)$$

In the case of weakly coupled model, we distinguish between the torsion angles in linear and branched fragments of the molecule. These are characterized by different sets $\{C_0 : C_1 : C_2 : C_3\}$ of values: $\{1.39 : 2.79 : 0.188 : -4.37\}$ and $\{0.515 : 1.27 : 0.370 : -2.40\}$ (in units of 10^{-20} J) for linear and branched fragments, respectively. These parameters are taken from the paper of Vlugt *et al.*[60] for branched alkanes and have been used in some of our previous studies.[50,58] The set of different values $\{1.79 : 5.57 : 1.38 : -8.74\}$ (in units of 10^{-20} J) is used for all torsion angles of the strongly coupled model. The shape of all torsion interactions is visualized in Fig. 3. Other bonded interactions are summarized elsewhere[58] and are not repeated here.

The photoisomerization of azobenzene is a complex quantum mechanical phenomenon which involves excitation of the electrons of the $N = N$ double bond and takes place on the time scale of tens of picoseconds.[27] However, given a scale of the force field modeling employed here, one can reduce it to the same classical mechanical level. It is assumed here that the material contains azobenzene chromophores with such chemical substituents (e.g., NO_2) that continuous cyclic *trans-cis* isomerization occurs at certain wavelength of the illumination. As far as the rate of the *trans-cis* photoisomerization is proportional to $\cos^2(\theta_i)$ (θ_i is the angle between the long axis of the ith *trans*-isomer and the light polarization), the *trans*-isomers are to be found predominantly perpendicular to the light polarization (orientational hole-burning effect). On the classical mechanical level this effect can be modeled by introducing the reorienting field which acts on each ith *trans*-isomer. The corresponding energy reads

$$U_{\rm i}^{\rm field}(\theta_{\rm i}) = F \cdot P_2(\cos(\theta_{\rm i})). \quad (2)$$

Here, the field strength is $F > 0$, (we will use the reduced field strength, f, where $F = f \cdot 10^{-20}$ J), $\theta_{\rm i}$ is the angle between the long axis of the ith *trans*-azobenzene and the direction of the field, and $P_2(x) = 1/2(3x^2 - 1)$ is the second Legendre polynomial. The derivative of $U_{\rm i}^{\rm field}(\theta_{\rm i})$ with respect to $\theta_{\rm i}$ is related to the torque acting on the ith azobenzene. One should note that, while both electric and magnetic fields align the azobenzenes uniaxially, the model field defined via Eq. (2) with $f > 0$ forces azobenzenes to stay preferentially in the plane perpendicular to the field direction. The latter can be associated with the polarization of the beam.

The aim of this study is to find the most relevant mechanisms for the photo-induced deformations and, therefore, some aspects of the photoisomerization are not considered. These are, in particular, the presence of *cis*-isomers and the kinetics of the photostationary state. The only effect being taken into account is the reorientation of the *trans*-isomers of the azobenzenes when the material approaches the photostationary state. Throughout this study, however, we discuss possible relevance of the *cis*-isomers in each particular case.

A few remarks should be made concerning the model density and the model temperature. The occupation volumes of pseudo-atoms and, especially, the chromophores are rather approximate, as far as rather flat *trans*-azobenzene is modeled via the ellipsoid of revolution (the energy surfaces of the Gay-Berne potential are approximately of that shape[56]). Due to this difference in packing abilities of real and model chromophore (see, e.g., Ref. 61 and 62), the absolute values of density are not expected to match exactly these for the real azo-polymers. The same holds for the temperature which is defined via the kinetic energy of the pseudo-atoms and chromophores. Due to the approximations made in the model, it cannot provide an exact match to the real temperature at which some particular chemical compound would be measured experimentally.

The MD simulations are performed with the aid of the parallel program GBMOLDD.[63,64] A simulation box with periodic boundary conditions, which mimics the behavior of a volume element in a bulk, is used. We employed simplified Parrinello-Rahman method,[65] in which only the diagonal components of stress tensor are constrained. It is to be referred as $NP_{XX}P_{YY}P_{ZZ}T$ ensemble, the details are given elsewhere.[58] The pressure is set equal to the atmospheric pressure, $P = P_{atm}$, by constraining the diagonal elements of stress tensor to P_{XX}, P_{YY}, P_{ZZ}, respectively (all values are equal to $P_{atm}/3$). For the integration of the equations of motion we used the leap-frog algorithm, the RATTLE constraint have been applied for the integration of mesogens rotation (see, Ref. 64). The time step $\Delta t = 2$ fs was found to be acceptable for all production runs. The simulation times span from 35 ns to 120 ns and are in the range of 6–20× the typical reorientation times for the azobenzene groups, depending on the particular model and its phase.

III. SIMULATION OF PHOTO-INDUCED DEFORMATIONS IN LIQUID-CRYSTALLINE AZO-POLYMERS

The LC azo-polymers are normally used below the order-disorder transition, in a monodomain (nematic or smectic, induced by the surface anchoring or by external field) or in a polydomain phase. The photo-induced deformation of a monodomain sample can be studied directly by simulation of a small volume element in the ordered phase. In the case of a polydomain sample, it can be assumed that each domain will contribute towards the total deformation depending on its local director. The domains with their director parallel to the polarization vector will photoisomerize (and, hence, deform) the most, whereas the ones with their director in perpendicular direction will remain nearly unaffected. The most striking demonstration of this possibility is the selective bending of a polydomain azobenzene-containing elastomer depending on the direction of a polarization vector.[12] In this way, the case of a polydomain sample can, in principle, be reduced to the case of a monodomain volume element being considered for different angles between its local director and the polarization vector. Alternatively, the polydomain sample can be considered explicitly.

The structure and internal dynamics of both monodomain and polydomain smectic phases in a weakly coupled model were studied by two of us earlier.[58] Preliminary studies of the photo-induced deformations of a monodomain volume element were also performed.[50–52] Here, we will extend these findings by considering a wider range of the reduced field strength f in Eq. (2), and also by considering the case of a polydomain sample explicitly. These extensions also require performing much longer simulation runs than of those being performed in Refs. 50–52. The simulation box (which represents a volume element) contains a melt of 64 chains, this is 8896 polymer beads, and 640 azobenzenes in total. In the case of a monodomain volume element, the uniform model field (defined via Eq. (2)) of various reduced strength f was applied parallel to the azobenzenes director. In the case of a polydomain volume element, three separate runs were performed for each f value. In each of these runs, the field was directed along one of spatial axes, X, Y, or Z and the results were averaged over three runs.

Here, we will introduce the properties being measured in a course of the simulation. The global orientational order of azobenzenes is monitored via order parameters $S_{||}$ and S_2,

$$S_{||} = \langle P_2(\vec{e}_i \cdot \hat{f})\rangle, \quad S_2 = \langle P_2(\vec{e}_i \cdot \hat{n})\rangle, \tag{3}$$

where $\vec{e}_i$ is defined along the long axis of the ith azobenzene, $\hat{f}$ is the direction of the applied field, and $\hat{n}$ denotes the azobenzenes nematic director. All the vectors in Eq. (3) are unit vectors, $P_2(x)$ is the second Legendre polynomial and averaging is performed over all the azobenzenes. The $S_{||}$ measures orientational order of the azobenzenes along the field applied, whereas the S_2 is their scalar nematic order parameter defined in a standard way.[66] One should remark that these properties do not distinguish between truly isotropic systems (no local LC order) and polydomain systems (with local LC order). Here, we will refer to the systems for which both order parameters are close to zero as "isotropic."

Conformational properties and spatial arrangement of polymer backbones can be characterized by the components of the gyration tensor, defined for the kth molecule as

$$G^{[k]}_{\alpha\beta} = \frac{1}{N_{bb}} \sum_{i=1}^{N_{bb}} \left(r^{[k]}_{i,\alpha} - R^{[k]}_{\alpha}\right)\left(r^{[k]}_{i,\beta} - R^{[k]}_{\beta}\right), \tag{4}$$

where α, β denote Cartesian axes and $\vec{R}^{[k]}$ is the position of the center of mass of the kth backbone made of N_{bb} sites. This tensor can be subsequently averaged over all the backbones in the melt, $G_{\alpha\beta} = \langle G^{[k]}_{\alpha\beta}\rangle$, to provide a measure of average anisotropy in polymer backbones mass distribution. Following Ref. 58, we also consider two order parameters for the orientational order of the backbones defined in the same way as for the chromophores, Eq. (3). In this case, $\vec{e}_i$ denotes the direction of the long axis of the equivalent ellipsoid for the ith backbone obtained via diagonalization of the gyration tensor (4).

The reaction of the volume element on an internal stress can be monitored via simulation box dimensions, L_x, L_y, and L_z. As was mentioned in Sec. II, the thermodynamical ensemble employed here allows monitoring of anisotropic deformations. We must remark that the question arises, to which extent the deformation of the simulation box (which represents a volume element) maps the one of the macroscopic samples. It is related to the affinity property of the macroscopic deformation and the answer is "yes" for the solid or elastomer, and "no" for the case of simple liquid (where random fluctuations of the box shape may occur as in the case of an isotropic fluid[67]). In the case of a viscous melt of an azo-polymer, one can assume that affinity approximately holds if the chains diffusion during the simulation run does not exceed the distances comparable with the box dimensions.

A. Monodomain smectic

We use the monodomain smectic volume element well equilibrated at $T = 485$ K, which is just below T_{SI}

~ 490 K.[58] Both the azobenzenes director and applied reorientation field are directed along Z axis, initial values for both order parameters are equal to $S_{||} = S_2 \approx 0.75$. With no external field applied the phase is found to be stable for at least 120 ns with minimal fluctuations of the order parameter and of dimensions of the box. With application of the field, this arrangement becomes energetically unfavorable and a torque applied to each chromophore attempts to reorient it perpendicularly to the field. The rate of the reorientation depends on the field strength f but is also affected by coupling of the chromophores to the polymer matrix.

What kind of response of the polymer matrix can be expected? If the field is strong enough (large f), then the time scale of chromophores reorientation may become much shorter than typical relaxation times of the polymer matrix. In this case one, generally, expects development of the internal stress and deformation of the volume element. At small values of field strength f the time scales of both processes may become of the same order. Then, one may expect several scenarios: (a) reorientation of azobenzenes with no deformation of the polymer (due to stress relaxation); (b) monotonical deformation of the polymer over extended time interval, "in phase" with reorientation of chromophores; or (c) deformation of the polymer at similar time scale as for the moderately strong field case (phase transition-like changes).

In our previous study,[50] we found only two scenarios. On the time scale considered there, $t \sim 6$ ns, the smectic-isotropic transition was observed at field strength of $f \leq 0.2$ (the "weak field" scenario). In stronger field, $f \geq 1.0$, the sequence of smectic-isotropic-smectic transitions took place with the nematic director in the final phase perpendicular to the field direction[50] (the "strong field" scenario). In both cases, the polymer matrix reacted by contraction along the direction of the field. To clarify the scenario(s) at much weaker fields, essentially longer simulation runs are required, and these are performed in the current study.

As a result, we found that all the general findings obtained in Ref. 50 hold, but the threshold value of f^* for the "weak field" scenario is about one order of magnitude lower, $f^* \sim 0.02$, than was estimated previously in Ref. 50. Indeed, the typical "weak field" scenario is observed at field strengths as low as $f = 0.015-0.020$ (see results averaged over this interval marked (b) in Fig. 4). Unfortunately, these particular simulation runs cannot be prolonged due to the effect of "monolayering" of the simulation box, at which case the simulations are terminated. (The reason behind this shortcoming is that the $NP_{XX}P_{YY}P_{ZZ}T$ ensemble is not well suited for the simulation of the isotropic phases, where random fluctuations of the simulation box dimensions take place.[67]) The run with a very weak field, $f = 0.005$ turned up to be unaffected by this problem for more than 120 ns (curves (a) in Fig. 4). The smectic-isotropic phase transition takes place during time interval $t \sim [45-65]$ ns, after no apparent changes are observed for about 45 ns in the smectic phase, but the duration of the transition ($\sim$20 ns) is the same as for the case of higher field strengths $f = 0.015-0.020$. Therefore, fourfold reduction of the field strength has an effect of mere time shifting of the transition, but not changing its typical time scale.

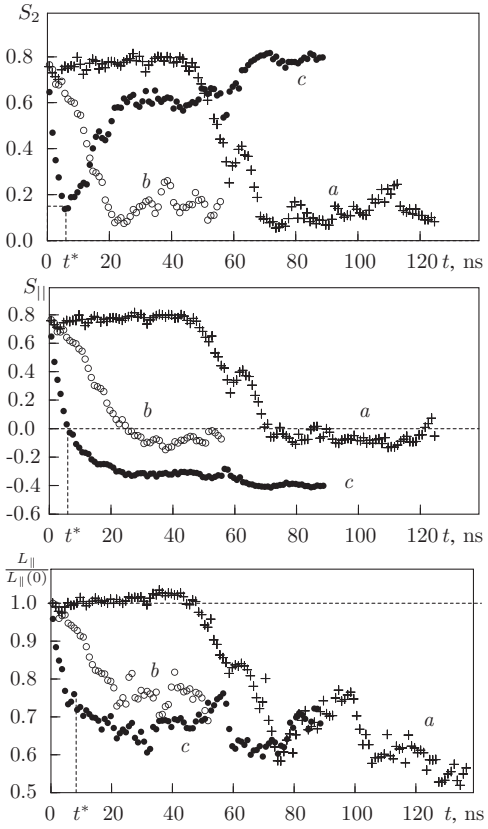

FIG. 4. Field-induced changes in the order parameters of azobenzenes, $S_{||}$ (topmost frame) and S_2 (middle frame) and in the reduced box dimension along the field, $L_{||}/L_{||}(0)$ (bottom image) for the monodomain smectic phase at $T = 485$ K ((a) curves – $f = 0.005$; (b) – the average over $f = 0.015$, $f = 0.017$, and $f = 0.020$ runs; (c) – the average over $f = 0.1$ and $f = 0.16$ runs).

The smectic-isotropic phase transition is accompanied by an essential contraction of the simulation box along the direction of the field, $L_{||}$, as shown in Fig. 4, bottom frame (curve a). We can conclude that, at least within a time window of 120 ns, we hit some interval of field strengths f for which the smectic-isotropic transition can be achieved solely due to the reorientation of *trans*-azobenzenes (with no formation of *cis*-isomers, as in the case of the real photochemical transition,[17,22–24]). Deformation of the box can be explained due to following considerations. The duration of the smectic-isotropic transition is about 20ns (the time interval $t \sim [45-65]$ ns in Fig. 4), and it is shorter than the estimated relaxation times for the chromophores reorientations in the equilibrium state, $\tau \approx 43$ ns.[58] As the result, the polymer is not given enough time to relax during the transition and the deformation of the polymer matrix takes place.

With the increase of f beyond $f \sim 0.020$ one observes the "strong field" scenario, in which two processes take place (see curves c in Fig. 4). The first process is the smectic-isotropic transition which takes place at $t < t^* \approx 5$ ns. It is followed by the second one, at $t > t^*$, during which the smectic phase is regrown with its director now being perpendicular to the field (relevant snapshots have been already published by us earlier[50]). Typical time scales of these transitions depend on the strength of the field, the data averaged over

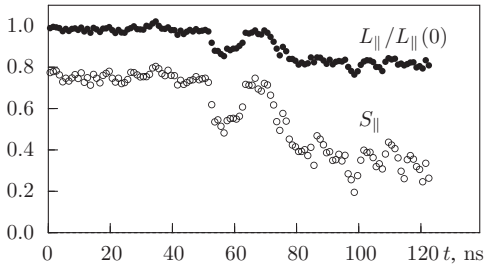

FIG. 5. Correlation between the order parameter $S_{||}$ and the reduced dimension of the box along the field, $L_{||}/L_{||}(0)$, during a pretransitional behavior observed during the run with $f = 0.007$.

$f = 0.1$ and $f = 0.16$ runs are shown in Fig. 4 (curve c). One can conclude that in the first process the field acts as a "melter" of the smectic phase and in the second as an aid for the self-assembly of the isotropic melt into the smectic phase. In this way, the "strong field" scenario combines both effects of photo-induced order-disorder transition and of the photo-alignment in azo-polymers.[15,23,24] Generally speaking, during the field-aided self-assembly the possibility of the planar phase exists, in which chromophores orientations are confined within the planes (perpendicular to the direction of the field) but with no orientational order within the planes. However, this phase is observed in none of the simulations being performed. The in-plane 2D symmetry is always broken in favor of the smectic layers.

One should stress that for the "strong field" scenario the anisotropic deformation of a volume element occurs only during the first process ($t < t^*$, smectic-isotropic transition), where $L_{||}$ decreases significantly. The second process, at ($t > t^*$, isotropic-smectic transition) takes place with no apparent systematic changes in simulation box dimensions. Therefore, the contraction of the volume element is reported for our model for both "weak field" and "strong field" scenarios. We can deduce that contraction of the smectic monodomain sample along the field is achieved primarily due to the destruction of the initial smectic order.

A strong correlation between the level of the LC order and the extension of the simulation box is clearly seen in Fig. 5, where the results of the simulation at $f = 0.007$ are shown. For this value of f, the melt is trapped in a long-living pretransitional ordered state characterized by the fluctuations of the order parameter. One observes remarkable synchronicity in the behavior of $S_{||}$ and $L_{||}$. One can deduce that the amount of the orientational order and the deformation of the box along the field are strongly coupled in this case.

One may conclude that the defining factor in contraction of the volume element along the field is the "randomization" of the azobenzenes orientations. The spacers are also known to align partially along the nematic director in smectic phase,[58] therefore these also add to the net effect. The contribution from the rearrangements of the backbones is also present in the deformation of the volume element observed as the result of the simulations. To clarify this point, we consider the components of their averaged gyration tensor $G_{\alpha\beta}$. In the isotropic phase $G_{\alpha\beta}$ is symmetric with all components close to $\approx 20\,\text{Å}^2$,[58] (square-rooted values are ≈ 4.47 Å). In

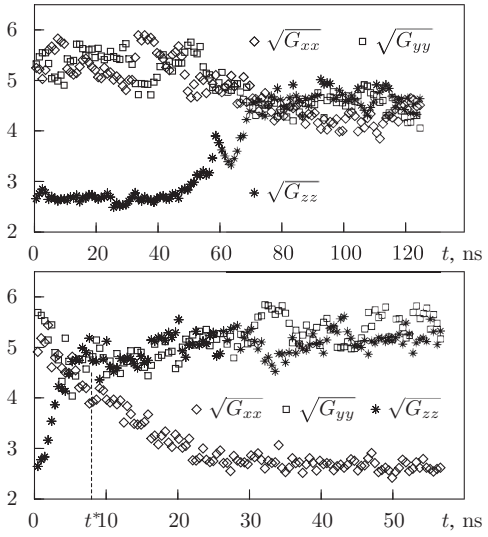

FIG. 6. Field-induced redistribution of polymer backbones mass during the $f = 0.005$ (top frame) and $f = 0.16$ (bottom frame) runs. Square-rooted components of the gyration tensor $G_{\alpha\alpha}$ in laboratory frame are shown.

the smectic phase $G_{\alpha\beta}$ is highly asymmetric, as the backbones are "sandwiched" in between the azobenzene layers.[58] Hence, the changes in $G_{\alpha\beta}$ components upon application of an external field, shown in Fig. 6, reflect the smectic-isotropic transition for "weak field" scenario (top frame) and the sequence of smectic-isotropic-smectic transitions for "strong field" scenario (bottom frame), as discussed above. The important point to mention here is that during the smectic-isotropic transition the backbones mass is redistributed along the field ($G_{zz} > \{G_{xx}, G_{yy}\}$). This effect "works" towards the extension of the volume element along the field, i.e., in an opposite direction to that of the azobenzenes. The net result is, however, contraction of the volume element, most likely, due to bulkiness of rigid azobenzenes, long spacers, and the flexibility of backbones in this model.

In the case of the field-induced isotropic-smectic transition ($t > t^*$ in Fig. 4), no systematic deformation is observed. One of possible explanation is that in this interval the contributions from the chromophores reorientation and from the backbones masses redistribution compensate each other. As a result, only the fluctuations of simulation box dimensions take place but not a systematic deformation. This behavior is closely related to the case of field-induced order in a polydomain volume element considered in the next subsection.

B. Polydomain smectic

The simulations discussed in this subsection are performed in a polydomain smectic phase prepared by quenching the isotropic phase with it subsequent equilibration at $T = 485$ K.[58] This phase contains randomly oriented smectic domains, but the global order is similar to that found in the isotropic phase. On the experimental side, such a sample can be turned into a monodomain by means of linearly polarized light.[15,23,24] In terms of optomechanical effects, photosensitive polydomain elastomer can be bended along the axis

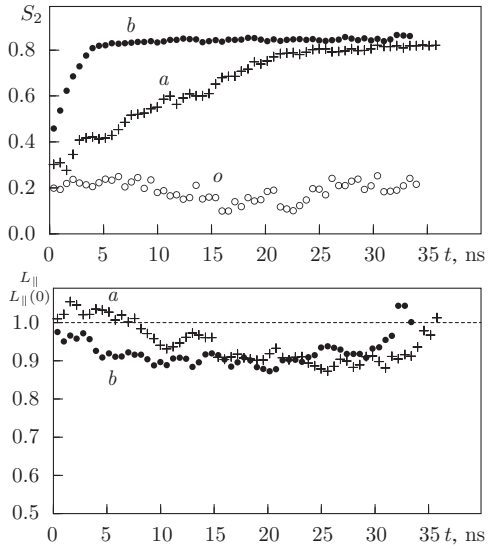

FIG. 7. Field-induced order parameter of azobenzenes S_2 (top frame) and box dimension along the field, $L_{||}$ (bottom frame) for the polydomain volume element of weakly coupled model. (o) denotes results at $f = 0$, (b) represents the average over $f = 0.2$, $f = 0.3$, and $f = 0.4$ runs, and (c) shows averaged data for $f = 0.5$, $f = 1$, and $f = 2$ runs.

defined by the polarization direction.[12,13] Our aim is to try to reproduce these effects in the simulations.

We cover the following range of field strengths: $f = 0.1-2.0$ and three simulations (with the field directed along X, Y, and Z axes) are performed for each f, the results of these are averaged. We found relatively large fluctuations of the simulation box dimensions, these can be attributed to a relatively small system size. As a consequence, the self-averaging of the properties of interest (typical for quenched random systems) is insufficient. One way to improve the statistics is to use a set of volume elements with different preparation history. Alternatively, we used the same initial volume element but performed averaging of the results obtained at close values of f. First set (marked on the figures as "a") is the average over $f = 0.2$, $f = 0.3$, and $f = 0.4$ runs, second one (marked as "b") stays for the average over $f = 0.5$, $f = 1.0$, and $f = 2.0$ runs. The run with zero field $f = 0$ is marked via "o." The results for the order parameter S_2 are shown in top frame of Fig. 7, these indicate a clear polydomain-monodomain transition with the nematic order parameter S_2 approaching value 0.8 at the end of the runs. The rate of the monodomain smectic growth depends on f. The evolution of the reduced simulation box dimension along the field, $L_{||}/L_{||}(0)$ is shown in the bottom frame of the same figure. It indicates a small drift which, however, cannot be interpreted as a systematic deformation of the simulation box.

This result supports similar findings obtained during the second process in the "strong field" scenario for the monodomain volume element discussed in a previous subsection (the time interval $t > t^*$ in Fig. 4). In both cases the initial phase is globally isotropic but has different preparation history (rapid field-induced smectic-isotropic transition and equilibrated quenched isotropic phase, respectively). This, however, makes no difference to the way the system responds on the reorientation of the azobenzenes.

The exact reason why the field-induced isotropic-smectic transition in a weakly coupled model takes place with no deformation of the volume element is difficult to prove without performing additional simulations. We see several possibilities as follows:

1. the choice of model parameters used here allows for the cancellation of two opposite tendencies: contraction due to reorientation of the azobenzenes and side chains and expansion due to the spatial redistribution of the backbones;
2. the effect is too delicate to be seen on the volume element size being considered here;
3. the effect requires more thorough configurational averaging.

The possibility 1 can be verified by simulation of a range of models with variable spacer length, backbone rigidity, etc. The possibilities 2 and 3 can, obviously, be verified by considering larger system sizes and a range of volume elements with different preparation path.

Brief conclusions to this section are given below. Both effects of photo-induced order-disorder transition and photo-induced alignment, observed experimentally in LC azo-polymers,[15,23,24] are reproduced using the mechanical model suggested in this study. For the monodomain smectic, the field is applied along the nematic director and the main opto-mechanical effect being observed is a strong coupling between the LC order and the extension of the volume element along the field. It leads to strong contraction in that direction during the field-induced smectic-isotropic phase transition. In this respect, the presence of *cis*-isomers will accelerate this transition further and it is expected that this opto-mechanical behavior will be preserved. For the polydomain smectic phase, the field induces a monodomain smectic phase, however, no systematic deformation is observed, in contrary to theoretical predictions[37] or experimental results.[12,13] Possible reason behind this result is either modeling (the deformations of opposite sign, related to chromophores and backbones rearrangements, cancel each other) or computational (insufficient system size) issue.

IV. PHOTO-INDUCED DEFORMATIONS IN AMORPHOUS AZO-POLYMERS

The strongly coupled model (see, Sec. II) is used to simulate photo-induced deformations in amorphous azo-polymers. In our simulations, 96 side-chain molecules are packed into the simulational box in a regular geometric way (5664 polymer beads and 960 azobenzenes in total). This configuration is first heated up to $T = 700$ K to erase the memory of the initial packing. After that the melt was cooled down to $T = 500$ K and equilibrated for 10 ns. To be able to relate the simulation temperatures to that of glass transition, T_g, we performed a rather brief simulation. This was done via step-by-step cooling of the melt within the temperature interval of $T \in [350\,\text{K}, 500\,\text{K}]$. Temperature was reduced in steps of 10–25 K by resetting it to a lower value and then allowing the system 4–8 ns to equilibrate. The glass transition temperature T_g is then estimated from the change of the slope in

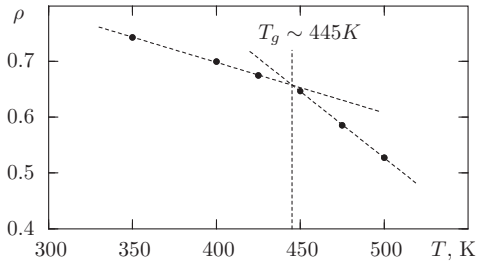

FIG. 8. Estimate of the glass transition temperature $T_g \sim 445$ K from the change of the density slope, strongly coupled model.

density-temperature plot, see Fig. 8, and found to lie between 440 K and 450 K.

We should remark here that a thorough study of the system behavior at and below T_g, as well as more precise estimate for T_g itself depending on cooling rate, is beyond the scope of this study. Otherwise, extremely long special purpose simulations and application of special technique would be required.[68] Besides that, the glass transition in polymer LC can be associated not only with the freezing up the torsion angles (as in ordinary polymer) but also with the strengthening of the LC interaction.

To look for the possibility for forming a monodomain nematic or smectic phase, we applied an external uniaxial aligning field, similar to the case of the weakly coupled model.[50,57,58] These attempts were unsuccessful and no stable monodomain ordered phases were found, in accordance with the typical phase diagrams of side-chain LC polymers with short spacer.[19–21] Instead, the polymer is found to adopt a polydomain LC phase, with strong intradomain LC interactions, which act as physical crosslinks.[69]

Most SRG inscriptions in amorphous systems are performed at $T < T_g$ aimed at fabrication of technologically desirable long-term stable gratings. However, the changes in the inscription process, when one approaches T_g may shed much light on relevant mechanisms of the process. It was shown in recent experiments[70,71] that under continuous exposure the grating height decays exponentially with the temperature increase and no permanent SRG can be recorded, if $T > T_g - 20\,^{\circ}$C. Although, under pulse-like exposure the grating still exists as long as the actinic light is on. It follows that at $T \sim T_g$, the SRG can be stable over short time interval, whereas subsequent stress relaxation prevents formation of a permanent grating.

We perform MD simulations both above the T_g and at $T \sim T_g$. All results presented in this section are obtained on macroscopically isotropic volume elements. As above, we perform three simulations at each field strength f (the field in each case was directed along X, Y, and Z axis, respectively) and average the results. In this way, we attempt to exclude the possibility when the effects being observed are related to the fluctuations. To improve the statistics further, in some cases, the averaging was also performed over the runs with close values of f.

A. Simulations at $T > T_g$

Here, we will discuss the results of the simulations performed at $T = 500\,\mathrm{K} > T_g$, where the melt has viscoelastic

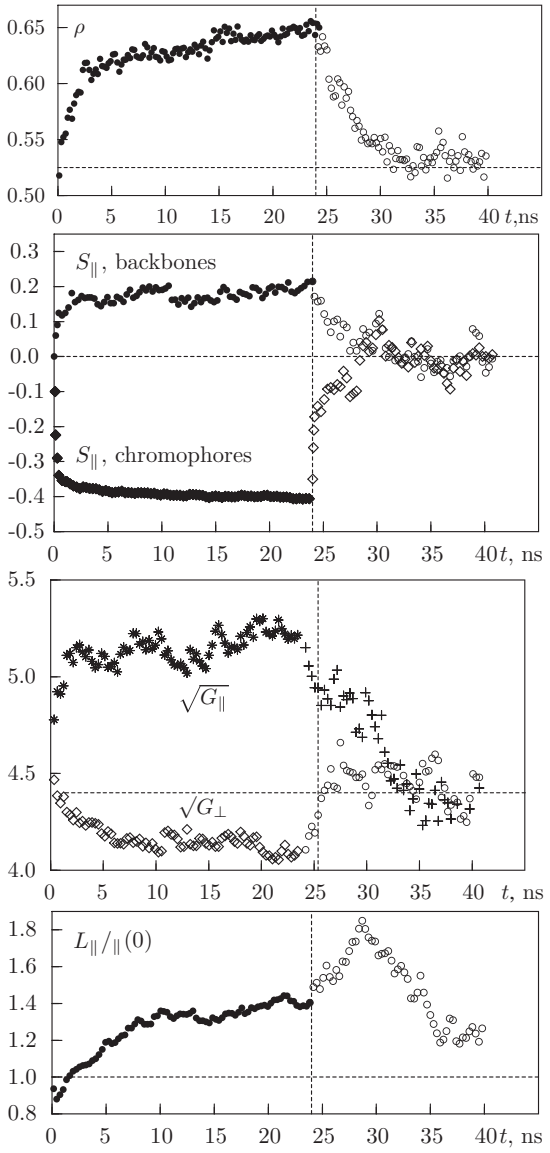

FIG. 9. Evolution of the density (top frame); of the order parameters along the field (second frame from the top); of the parallel and perpendicular squared components of the gyration tensor in respect to the field direction (third from the top); and of the dimensions of the box parallel and perpendicular to the field (bottom frame) upon application of the field with strength $f = 1.6$ at $t = 0$ and switching it off at $t = 24$ ns (the temperature is at $T = 500$ K).

properties. As was already found by us before in Refs. 51 and 52 at this temperature photo-induced deformations are observed only within a certain interval of values for the field strength, $f = 1 - 1.7$. Here, we will discuss the reason for this finding and also extend our study on the subject of reversibility of acquired deformation.

Let us consider the mechanical response of the melt upon application of the field with the strength $f = 1.6$ (Refs. 51,52) in more detail. The field is switched on at $t = 0$ and switched off at $t = 24$ ns. The evolution of density, order parameters, components of backbones gyration tensor, and the dimensions of the simulation box are shown in Fig. 9.

Upon application of the field, the first effect to mention is drastic growth of the density from $0.52\,\mathrm{g/cm^3}$ to about $0.65\,\mathrm{g/cm^3}$ (Fig. 9, top frame). In fact, the system is driven

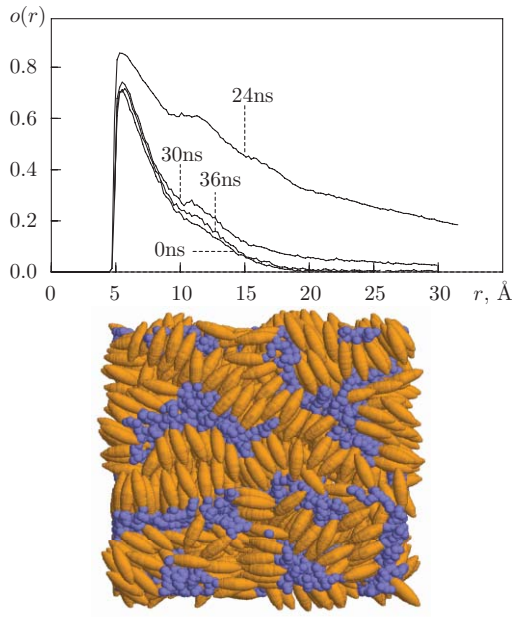

FIG. 10. Pair orientational correlation function at different time instances (for the references, see Fig. 9), top frame; and snapshot of the dense polydomain phase at $t = 24$ ns, bottom frame. Temperature is $T = 500$ K, field strength is $f = 1.6$.

by the field into the state with the density found at $T < T_g$ with no field applied (see, Fig. 8). This can be understood in terms of partial "orientational freezing" of chromophores by the field, which is redistributed over other degrees of freedom. Another confirmation of the effective "temperature shift" is much enhanced local LC order as indicated by a pair orientational correlation function $o(r)$ between ith and jth azobenzene,

$$o(r) = \langle P_2(\mathbf{e}_i \cdot \mathbf{e}_j)\rangle|_{r=r_{ij}}. \quad (5)$$

The curve for $o(r)$ raises up until a certain saturated profile is reached at $t = 20$–24 ns (Fig. 10, top frame). Increased local LC order is confirmed also by a snapshot shown in the bottom frame of the same figure. After the field is turned off, at $t = 24$ ns, the density reverts back to the initial value of $0.52\,\mathrm{g/cm^3}$ as well as the local order does (see, Figs. 9–10, top frames).

Similar to the case of the polydomain LC azo-polymer, considered in Sec. IV, the effect of photo-induced reorientation of chromophores is observed clearly. This is seen on the behavior of azobenzenes order parameter $S_{||}$ shown in Fig. 9, second frame from the top. The changes in the order parameter of the backbones (shown in the same figure) are found to take place on the same time scale, this indicates the reorientation of the molecule as a whole (due to strong coupling nature of this molecular architecture). Backbones reorientation is also confirmed by the anisotropy of their average gyration tensor (Fig. 9, third frame from the top). The $G_{||}$ component is about 20% larger than the $G_{\perp}$ one (at $t = 24$ ns). The isotropic case is restored after the field is switched off. One should note that the shapes of the curves for $G_{||}$ and $S_{||}$ are very similar.

It is very important to note that the same principal structural changes (reorientation of the chromophores and backbones perpendicularly and parallel to the field, respectively) are observed as in the case of LC azo-polymer. However, the mechanical response of the polymer is opposite, the volume element extends about 140% along the field (Fig. 9, bottom frame). One can conclude that the contribution from the backbones reorientations to the stress is more essential than that from the reorientation of chromophores. This can be attributed to backbones stiffness and to a short spacer which is characteristic for the strongly coupled model considered in this section.

Now, we would comment on the behavior of the azo-polymer after the field is switched off (time interval $t > 24$ ns in Fig. 9). In $10-15$ ns time, the field-induced state of the polymer reverts back to almost the initial state. In particular, the order parameter of backbones along the field $S_{||}$ is lost and the dimension of the volume element in the same direction $L_{||}$ undergoes certain changes, shown in the bottom frame of Fig. 9. To understand the behavior of the volume element reduced dimension $L_{||}/L_{||}(0)$, one should turn attention to the evolution of the density, Fig. 9 (top frame). At the first stage, $t = 0-24$ ns, the ordering of backbones dominates and the box extends along the field. At the second stage, when the field is just turned off, $t = 24-30$ ns, the order of backbones decreases, but the box continues to extend. This might be attributed to the rapid decrease of the density occurring at this stage. Finally, at the third stage, $t > 30$ ns, the melt returns to almost initial state with no backbones order being driven by the elastic forces and, possibly, by thermal fluctuations. Some residual deformation persists, though, due to viscoelasticity of the melt.

In this way, it became clear that the field applied at $T = 500\mathrm{K} > T_g$ has an effect of driving the model azo-polymer to the state similar to that observed below T_g. In this state the density is higher, and this change promotes higher coupling between the reorientations and mechanical stress. On the other hand, the increased local liquid crystallinity results in formation of physical crosslinks[69] which blocks the deformation. In a weak field, the coupling between the reorientations and the stress is insufficient and no deformation is observed, whereas in a high field the deformation is blocked by a local LC order.[51,52] Good compromise between two opposite effects must have been achieved in some interval of intermediate field strength, including the case of $f = 1.6$ considered above.

One may conclude that at $T > T_g$ the modeled photo-induced deformations are much hindered by essential changes in both density and local LC order. To reduce the influence of these factors, one can attempt performing simulations closer or even below the T_g temperature. In this case, the density is higher and the coupling between the molecular reorientations and mechanical stress is enhanced. As the result, one might expect that the photo-induced deformations can be induced at far lower field strengths f. This conclusion is supported by our simulations performed at $T \sim T_g$ that are discussed in the following subsection.

B. Simulations at $T \sim T_g$

Most SRG inscriptions in amorphous azo-polymers are performed well below $T < T_g$, but the required time scales

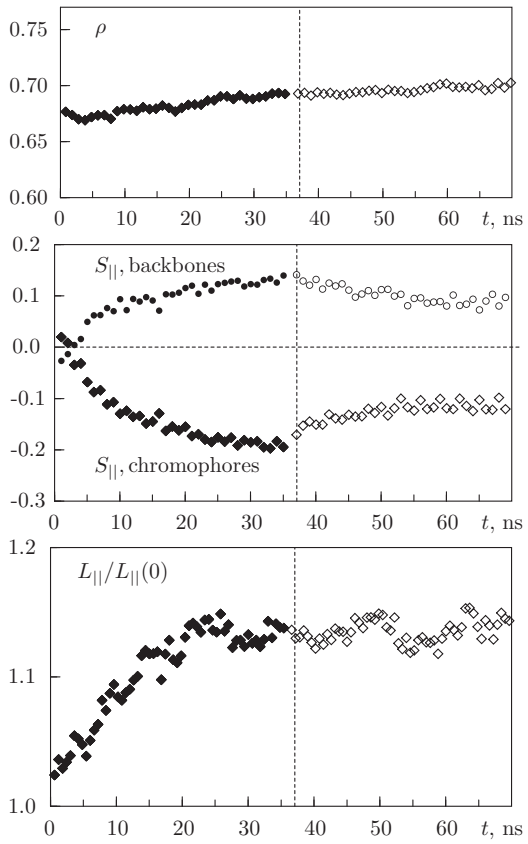

FIG. 11. Evolution of the density (top frame); of the order parameters along the field (second frame from the top); and of the dimensions of the box parallel and perpendicular to the field (bottom frame) upon application of the field at $t = 0$ and switching it off at $t = 37$ ns. The temperature is $T = 450$ K and the data are averaged over the runs with the field strengths $f = 0.15, 0.2, 0.5$.

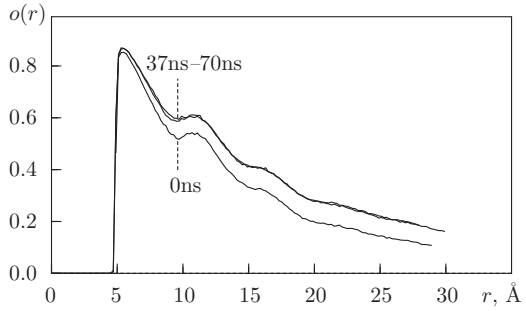

FIG. 12. Pair orientational correlation function at different time instances (for the references, see Fig. 11). Temperature is $T = 450$ K, data are averaged over $f = 0.15, 0.2, 0.5$ runs.

are difficult to cover via MD simulations. Therefore, we performed another set of simulations at $T \sim T_g$ targeted to reveal certain tendencies for the photo-induced deformations that occur at reduction of the temperature and could be extrapolated further to $T < T_g$ region. As already mentioned above, at $T \sim T_g$ we expect a better coupling between the molecular reorientation and mechanical stress in the melt as compared to the $T > T_g$. On the other hand, the elasticity is much suppressed, therefore one expects non-reversible changes in polymer structure and, therefore, permanent deformation of the sample after the field is switched off.

Simulations are performed at T = 450 K which is close to the estimate for $T_g \approx 445$ K made from Fig. 8. Well equilibrated configuration was prepared by cooling the melt from $T = 500$ K down to $T = 450$ K and by subsequent equilibration for relatively long time of 65 ns. Similar to the case of $T = 500$ K, the external field of different strength was applied in turn along each spatial axis and the results were averaged over three runs. The effect of photo-induced deformation was observed in a range of $f \sim 0.1-0.7$, and these values are essentially lower than $f \sim 1$ required in the case of $T = 500$ K. This confirms the idea expressed above that at higher density the deformation of a volume element can be observed at lower field strength f, in accordance with the experiment.

All properties of interest are found to behave quite similarly for $f = 0.15$, 0.20, and 0.50 field strengths (here one can ignore small differences in reorientation dynamics in this interval of values of f); and therefore, the results are averaged over these runs to improve statistics. The data are shown in Fig. 11. The shortcomings of the simulations at $T = 500$ K are found to be overcame at $T = 450$ K. First of all, no essential density change is observed as the result of application of the field (see, Fig. 11, top frame). One reason for this is much lower strength of the field f, hence it induces the changes that are equivalent to relatively small reduction of the temperature, if no field is present (see discussion in a previous subsection). This is indicative that the overall structure of a system does not change essentially upon application of the field and this conclusion is also supported by only subtle changes in the shape of the pair orientational correlation function $o(r)$ upon application of the field (see, Fig. 12).

The changes in orientational order parameters for chromophores and backbones acquired due to application of the field are found to be stable after the field is switched off (at $t = 37$ ns) for at least another 30 ns (Fig. 11, middle frame). This is in a sharp contrast to the case of $T = 500$ K, when the order vanishes in about 5 ns after the field is switched off (Fig. 9). The same holds true also for the dimension of the volume element along the field, $L_{||}$, which is found to behave smoothly with no "kick" after the field is switched off. The expansion of the box acquired along the applied field is preserved for at least another 30 ns after the field is switched off (Fig. 11, bottom frame). More precise determination of the stability of field-induced deformation requires much longer simulation runs which, in turn, needs a simulation box of a larger size. The reason for this is that the film can turn into a monolayer in one of dimensions perpendicular to the field ($L_\perp$) due to spontaneous shape fluctuations.

Let us consider again the possible role of the *cis*-isomers, if being taken into account explicitly. Their presence will dilute and, therefore, lessen the local LC ordering and decrease the role of physical crosslinks, the effect that prevents mechanical changes at higher values of field f. Otherwise, the *cis*-isomers will decrease the net torque applied on each molecule which may result in a need for stronger fields to be applied or longer time to achieve the deformation. In any case, the basic mechanism is expected to hold on.

The results obtained at both $T > T_g$ and $T \sim T_g$ provide an evidence for the following microscopic mechanism for photo-induced deformations in a strongly coupled model.

First of all, due to the strong coupling between chromophores and backbones, the molecules behave similar to rigid bodies (the time scale of the order parameter evolution for both chromophores and backbones is the same). Given suitable conditions, these massive molecular reorientations lead to the build-up of anisotropic internal stress, which causes temporary or permanent deformation of the volume element. In the case of $T > T_g$ the deformation is observed at moderately large field strengths, $f = 1 - 2$, in which case the system is driven first to the state with higher density (typical for the temperature range $T < T_g$). The deformations are temporal, as far as, upon switching the field off the system reverts back to almost initial (pre-field) state. This process is driven by the elasticity of the melt and is aided by thermal fluctuations and reduced density after the field is switched off. At weaker fields, $f < 1$, no deformation is observed (most likely due to insufficient density increase), and at high fields, $f > 2$ it must be blocked by greatly enhanced local LC order. In the case of temperatures $T \sim T_g$, the initial density of the melt is essentially higher and the internal stress (and, consequently, anisotropic deformation) is developed at much weaker fields, $f = 0.1-0.7$, and stays permanent during at least the simulation time of 30 nsperformed in this study. The sign of the deformation (extension of the volume element along the field direction) points out on the role of backbone rigidity, as far as the effect of backbones reorientation wins over the effect of chromophores reorientation perpendicularly to the field.

In the case of amorphous polymer (stiff backbone, short spacer), the effect of backbones reorientation is prevailing and the volume element is found to extend along the applied field. In this study, we performed simulations both at $T > T_g$ and at $T \sim T_g$. At $T > T_g$, the deformation is observed at moderately large strengths of the reorientation field as the melt is driven first to the state with higher density. At $T \sim T_g$, the initial density is much higher as at $T > T_g$ and the deformation of the volume element is induced at much weaker fields. The deformation of the polymer was found to be reversible at $T > T_g$ and irreversible (at least at the time scale of our simulations) at $T \sim T_g$. The result agrees qualitatively with recent experiments on temperature dependence of pulse recording of the surface reliefs.[70,71]

The main result of this study is the unambiguous demonstration that opposite photo-induced deformations, observed experimentally on liquid crystalline and amorphous polymers, can be explained solely on the basis of molecular reorientations initiated by orientational hole burning effect. For both molecular architectures, chromophores orient perpendicularly and backbones orient parallel in respect to the external field (which direction is associated with the polarization vector). These reorientations compete in terms of volume element deformation, as far as chromophores reorientation promote contraction, whereas that of the backbones promote extension along the direction of the field. The final result depends, therefore, on subtle details of molecular architecture.

V. CONCLUSIONS

We performed extensive molecular dynamics simulations of two models representing, in an effective way, the photo-induced deformations of the azobenzene containing polymers. Both liquid crystalline and amorphous azo-polymers are modeled as a side-chain architecture but with different amount of coupling between the backbone and pending chromophores and different rigidity of the backbone. The united-atom force field modeling was used for the polymer subsystem and the photoisomerization of azobenzenes was considered on a level of the orientational hole burning effect, via introducing an external reorientating field. We consider a volume element of the material which is represented via a molecular dynamics simulation box.

We found that in the case of the liquid crystalline polymer (flexible backbone, longer spacer), the reorientation of the side groups contributes the most to the net effect of volume element deformation. This is seen the most prominently in the case of a monodomain smectic phase. If the weak field is applied along the initial nematic director, then the material undergoes a field-induced smectic-isotropic transition and contracts along the field direction. The same type of deformation is preserved in strong fields, in which case the smectic-isotropic transition is followed by field-induced isotropic-smectic transition. No systematic deformation is observed for the case of a macroscopically isotropic polydomain sample. We see the reason for this observation in either the compensation of two effects originating from the reorientation of azobenzenes and polymer backbones or due to insufficient system size.

ACKNOWLEDGEMENTS

The authors acknowledge financial support under German Research Foundation (DFG) Grant Nos. NE410/8-2 and GR 3725/2-1. J. I. thanks to O. Kulikovska and J. Stumpe for stimulating discussions.

[1] D. Sainova, A. Zen, H.-G. Nothofer, U. Asawapirom, U. Scherf, R. Hagen, T. Bieringer, S. Kostromine, and D. Neher, Adv. Funct. Mater. **12**, 49 (2002).
[2] A. Zen, D. Neher, C. Bauer, U. Asawapirom, U. Scherf, R. Hagen, S. Kostromine, and R. F. Mahrt, Appl. Phys. Lett. **80**, 4699 (2002).
[3] N. K. Viswanathan, D. Y. Kim, S. Bian, J. Williams, W. Liu, L. Li, L. Samuelson, J. Kumar, and S. K. J. Tripathy, Mater. Chem. **9**, 1941 (1999).
[4] A. Natansohn and P. Rochon, Adv. Mater. **11**, 1387 (1999).
[5] R. H. Berg, S. Hvilsted, and P. S. Ramanujam, Nature (London) **383**, 505 (1996).
[6] P. H. Rasmussen, P. S. Ramanujam, S. Hvilsted, and R. H. Berg, J. Am. Chem. Soc. **121**, 4738 (1999).
[7] S. J. Zilker, T. Bieringer, D. Haarer, R. S. Stein, J. W. van Egmond, and S. G. Kostromine, Adv. Mater. **10**, 855 (1998).
[8] A. Stracke, J. H. Wendorff, D. Goldmann, D. Janietz, and B. Stiller, Adv. Mater. **12**, 282 (2000).
[9] B. Stiller, T. Geue, K. Morawetz, and M. Saphiannikova, J. Microsc. **219**, 109 (2005).
[10] H. Finkelmann, E. Nishikawa, G. G. Pereira, and M. Warner, Phys. Rev. Lett. **87**, 015501, (2001).
[11] M. Camacho-Lopez, H. Finkelmann, P. Palffy-Muhoray, and M. Shelly, Nat. Mater. **3**, 307 (2004).
[12] Y. L. Yu, M. Nakano, and T. Ikeda, Nature (London) **425**, 145 (2003).
[13] T. Ikeda, J. Mamiya, and Y. Yu, Angew. Chem., Int. Ed. **46**, 506 (2007).
[14] O. N. Oliveira Jr., J. Kumar, L. Li, and S. K. Tripathy, in *Photoreactive Organic Thin Films*, edited by Z. Sekkat and W. Knoll (Elsevier, New York, 2002), p. 560.
[15] K. Ichimura, Chem. Rev. **100**, 1847 (2000).
[16] S. Hvilsted and P. S. Ramanujam, Monatsh. Chem. **132**, 43 (2001).

[17]C. J. Barrett, J. Mamiya, K. G. Yager, and T. Ikeda, Soft Matter **3**, 1249 (2007).
[18]H. Rau, in *Photoisomerization of Azobenzenes*, edited by J. Rebek (CRC, Boca Raton, FL, 1990).
[19]P. J. Collings and M. Hird, *Introduction to Liquid Crystals* (Taylor & Francis, London, 2001).
[20]M. Rutloh, J. Stumpe, L. Stachanov, S. Kostromin, and V. Shibaev, Mol. Cryst. Liq. Cryst. **352**, 149 (2000).
[21]S. Freiberg, F. Lagugné-Labarthet, P. Rochon, and A. Natansohn, Macromolecules **36**, 2680 (2003).
[22]T. Ikeda, S. Horiuchi, D. B. Karanjit, S. Kurihara, and S. Tazuke, Macromolecules **23**, 42 (1990).
[23]T. Ikeda, S. Yoneyama, T. Yamamoto, and M. Hasegawa, Mol. Cryst. Liq. Cryst. **375**, 45 (2002).
[24]T. Ikeda, J. Mater. Chem. **13**, 2037 (2003).
[25]M. Eich, J. H. Wendorff, B. Reck, and H. Ringsdorf, Macromol. Rapid Commun. **8**, 59 (1987).
[26]T. Todorov, L. Nikolova, and N. Tomova, Appl. Opt. **23**, 4309 (1984).
[27]J. Michl and E. W. Thulstrup, Spectroscopy with Polarized Light (VCH, New York, 1995), p. 198.
[28]A. Natansohn, P. Rochon, J. Gosselin, and S. Xie, Macromolecules **25**, 2268 (1992).
[29]L. Läsker, J. Stumpe , T. Fischer, M. Rutloh, S. Kostromin, and R. Ruhmann, Mol. Cryst. Liq. Cryst. **261**, 371 (1995).
[30]D. Bublitz, M. Helgert, B. Fleck, L. Wenke, S. Hvilstedt, and P. S. Ramanujam, Appl. Phys. B **70**, 863 (2000).
[31]N. C. R. Holme, L. Nikolova, S. Hvilsted, P. H. Rasmussen, R. H. Berg, and P. S. Ramanujam, Appl. Phys. Lett. **74**, 519 (1999).
[32]P. Rochon, E. Batalla, and A. Natansohn, Appl. Phys. Lett. **66**, 136 (1995).
[33]D. Y. Kim, S. K. Tripathy, L. Li, and J. Kumar, Appl. Phys. Lett. **66**, 1166 (1995).
[34]C. J. Barrett, P. L. Rochon, and A. Natansohn, J. Chem. Phys. **109**, 1505 (1998).
[35]J. Kumar, L. Li, X. L. Jiang, D. Y. Kim, T. S. Lee, and S. Tripathy, Appl. Phys. Lett. **72**, 2096 (1998).
[36]P. Lefin, C. Fiorini, and J.-M. Nunzi, Pure Appl. Opt. **7**, 71 (1998).
[37]T. G. Pedersen, P. M. Johansen, N. C. R. Holme, P. S. Ramanujam, and S. Hvilsted, Phys. Rev. Lett. **80**, 89 (1998).
[38]O. Baldus and S. Zilker, J. Appl. Phys. B **72**, 425 (1998).
[39]D. Bublitz, B. Fleck, and L. Wenke, Appl. Phys. B **72**, 931 (2001).
[40]Y. B. Gaididei, P. L. Christiansen, and P. S. Ramanujam, Appl. Phys. B **74**, 139 (2002).
[41]M. Saphiannikova, T. M. Geue, O. Henneberg, K. Morawetz, and U. Pietsch, J. Chem. Phys. **120**, 4039 (2004).
[42]M. Saphiannikova and D. Neher, J. Phys. Chem. B **109**, 19428 (2005).
[43]N. Mechau, D. Neher, V. Bürger, H. Menzel, and K. Urajama, Appl. Phys. Lett. **81**, 4715 (2002).
[44]N. Mechau, M. Saphiannikova, and D. Neher, Macromolecules **38**, 3894 (2005).
[45]V. Toshchevikov, M. Saphiannikova, and G. Heinrich, J. Phys. Chem. B **113**, 5032 (2009).
[46]R. Barillé, P. Tajalli, S. Kucharski, E. Ortyl, and J.-M. Nunzi, Appl. Phys. Lett. **96**, 163104 (2010).
[47]S. Ahmadi-Kandjani, R. Barillé, S. Dabos-Seignon, J. M. Nunzi, E. Ortyl, and S. Kucharski, Opt. Lett. **30**, 3177 (2005).
[48]O. Henneberg, T. M. Geue, M. Saphiannikova, U. Pietsch, P. L. Rochon, and A. Natansohn, Appl. Surf. Sci. **182**, 272 (2001).
[49]W. Maier and A. Saupe, Z. Naturforsch. **14**, 882 (1959).
[50]J. Ilnytskyi, M. Saphiannikova, and D. Neher, Condens. Matter Phys. **9**, 87 (2006).
[51]J. M. Ilnytskyi, D. Neher, M. Saphiannikova, M. R. Wilson, and L. M. Stimson, Mol. Cryst. Liq. Cryst. **496**, 186 (2008).
[52]J. M. Ilnytskyi, D. Neher, and M. Saphiannikova, in *CP1091, Modeling and Simulation of New Materials: Tenth Granada Lectures*, edited by P. L. Garrido, P. I. Hurtago, and Joaquin Marro (AIP, Melville, NY, 2009).
[53]M. Saphiannikova, V. Toshchevikov, and J. Ilnytskyi, Nonlinear Opt., Quantum Opt. **41**, 27 (2010).
[54]M. R. Wilson, J. Chem. Phys. **107**, 8654 (1997).
[55]C. McBride and M. R. Wilson, Mol. Phys. **97**, 511 (1999). M. R. Wilson, J. M. Ilnytskyi, and L. M. Stimson, J. Chem. Phys. **119**, 3509 (2003). M. R. Wilson, J. M. Ilnytskyi, L. M. Stimson, and Z. E. Hughes, in *Computer Simulations of Liquid Crystals and Polymers*, edited by P. Pasini, C. Zannoni, and S. Zumer, (Kluwer, Dordrecht, 2004), p. 57.
[56]J. G. Gay and B. J. Berne, J. Chem. Phys. **74**, 3316 (1981).
[57]L. M. Stimson and M. R. Wilson, J. Chem. Phys. **123**, 034908 (2005).
[58]J. M. Ilnytskyi and D. Neher, J. Chem. Phys. **126**, 174905 (2007).
[59]J. P. Ryckaert and A. Bellemans, Chem. Phys. Lett. **30**, 123 (1990).
[60]T. J. H. Vlugt, R. Krishna, and B. Smit, J. Phys. Chem. B **103**, 1102 (1999).
[61]G. L. Penna, D. Catalano, and C. A. Veracini, J. Chem. Phys. **105**, 7097 (1996).
[62]A. Cuetos, J. M. Ilnytskyi, and M. R. Wilson, Mol. Phys. **100**, 3839 (2002).
[63]J. Ilnytskyi and M. R. Wilson, Comput. Phys. Commun. **134**, 23 (2001).
[64]J. Ilnytskyi and M. R. Wilson, Comput. Phys. Commun. **148**, 43 (2002).
[65]M. Parrinello and A. Rahman, J. Appl. Phys. **52**, 7182 (1981).
[66]P. G. de Gennes and J. Prost, *The Physics of Liquid Crystals*, 2nd ed. (Oxford University Press, New York, 1995).
[67]M. P. Allen and D. J. Tildesley, *Computer Simulation of Liquids* (Clarendon, Oxford, 1987) (Reprinted 1991).
[68]J. Han, R. H. Gee, and R. H. Boyd, Macromolecules, **27**, 7781 (1994); A. V. Lyulin, N. K. Balabaev, and M. A. J. Michels, Macromolecules **36**, 8574 (2003).
[69]J. L. Gallani, L. Hilliou, P. Martinoty, and P. Keller, Phys. Rev. Lett. **72**, 2109 (1994).
[70]P. U. Veer, U. Pietsch, P. L. Rochon, and M. Saphiannikova, Mol. Cryst. Liq. Cryst. **486**, 66 (2008).
[71]P. U. Veer, U. Pietsch, and M. Saphiannikova, J. Appl. Phys. **106** 014909 (2009).